Proton-implantation-induced defects in *n*-type 6*H*- and 4*H*-SiC: An electron paramagnetic resonance study

H. J. von Bardeleben, J. L. Cantin, and I. Vickridge
Groupe de Physique des Solides, Universités Paris 6&7, UMR 75-88 du CNRS, 2, Place Jussieu, 75251 Paris, France

G. Battistig
MTA-Research Institute for Technical Physics and Materials Science, H-1525 Budapest, Hungary

(Received 5 May 2000)

The microscopic structure and introduction rate of point defects in *n*-type 6H- and 4H-SiC generated by room-temperature proton implantation have been studied by the electron paramagnetic resonance technique. In order to selectively study the effects of defect introduction in the trace region, 12-MeV implantation in 300-μm-thick samples was employed, for which the protons completely cross the sample. In both polytypes we observe three dominant paramagnetic defects attributed to the Si monovacancy in the negative charge state and the neutral Si monovacancy in the hexagonal and quasicubic lattice sites, respectively. The concentration of all three defects increases linearly with proton dose. Their total introduction rate is $\sim$19 cm^{-1}, which amounts only to 4% of the concentration expected from SRIM simulations. No carbon-vacancy-related defect is observed. Thermal annealing at 1100 °C is sufficient to anneal out the V_{Si} defects and to restore *n*-type conductivity. The observation of the neutral Si vacancy at hexagonal and quasicubic sites under thermal equilibrium conditions at 4 K does not support their previous assignment to an excited state.

INTRODUCTION

Ion implantation in SiC (Refs. 1 and 2) is widely used for *n* and *p*-type doping (N and Al implantation), and for splitting epitaxial layers from their substrate (proton implantation) in the smart cut process[3] employed in SiC on insulator technology. Doping by implantation requires, in addition to the electrical activation of the dopant, a thermal annealing of the implantation related intrinsic point or extended defects, which were found to strongly reduce the electrical conductivity. Whereas in silicon both can be achieved by thermal annealing in the 800 °C range with an almost complete elimination of the induced point defects, the different material properties of SiC render the use of ion implantation much more difficult. This is especially related to an increased defect stability and the existence of various polytypes. Also, in noncubic polytypes, more complex crystal structures—as compared to Si—introduce nonequivalent lattice sites with site-dependent defect properties. In the 6H polytype, for example, three nonequivalent Si and C sites exist, which, according to their second-nearest-neighbor coordinations are called quasicubic1 ($c1$), quasicubic2 ($c2$), and hexagonal (h). The electronic properties of substitutional point defects such as the dopants[4] N and Al or the transition metals[5] Voh, Mo,[6] strongly depend on the ($c1$,$c2$,h) site location. The bond lengths in 6H-SiC are shorter than in Si—1.88 Å as compared to 2.35 Å—and their strengths are increased: 3.2 eV as compared to 2.35 eV in Si. Thus higher energies are required to displace an atom from its lattice site: 14 eV in the case of Si and (20,...,30) eV in the case of SiC. The exact value is still a matter of debate for SiC.[2,7] The higher displacement energies further lead to an increased stability of the implantation induced intrinsic defects and in SiC temperatures above 1300 °C are required for their annealing, with a complete recovery of the electrical conductivity requirings anneals at even higher temperatures. These problems are a serious impediment to the development of SiC devices, and an improved understanding of the basic processes that occur during ion implantation is an essential step for further progress.

Ion implantation in covalent semiconductors is accompanied by the formation of intrinsic point defects due to elastic collision processes between the ion and lattice atoms. For high ion energies the energy loss is almost entirely to target electrons, whereas in the low-energy regime atomic collisions with vacancy cascade formation prevail. The density of point-defect formation in the region near the end of the ion range is thus much higher than in the rest of the ion track, which we refer to as the trace region. This is illustrated of Fig. 1, where we show the generation of primary defects calculated with the SRIM2000.39 Monte Carlo code[8] as a function of depth for 12-MeV protons. Note that the SRIM2000 code does not take into account recombination of the primary interstitials and vacancies—and so residual damage levels can be lower. Because of the much lower primary defect production rate in the trace, monovacancies or divacancies would be expected to dominate there, with vacancy clusters near the end of range, but the real nature of the implantation-induced defects is still far from clear.

In this work we focus on the nature and concentration of the trace defects generated by proton implantation in 6H- and 4H-SiC. The microscopic structure of the proton implantation related intrinsic defects in SiC is still uncertain. Various defects have been evidenced in ion-implanted SiC by photoluminescence[9–11] electrical measurements,[12,13] positron lifetime analysis,[14,15] and electron paramagnetic (EPR) spectroscopy.[16–18] Divacancy defects and extended vacancy clusters are generally believed to be the dominant defects in nonamorphized material, but clear evidence of their attribu-

0163-1829/2000/62(15)/10126(9)/$15.00 PRB 62 ©2000 The American Physical Society

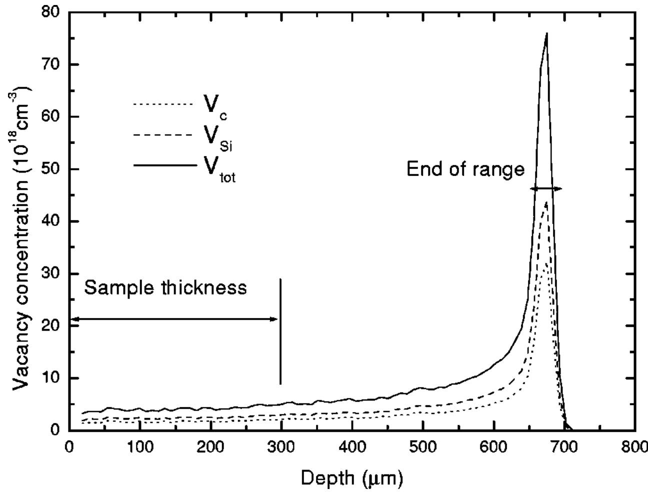

FIG. 1. Volume concentrations of carbon and silicon vacancies and their sum generated by the implantation of $1\times10^{16}\,\mathrm{cm}^{-2}$ 12 MeV protons in 6H-SiC as a function of target depth determined by SRIM2000 simulations.

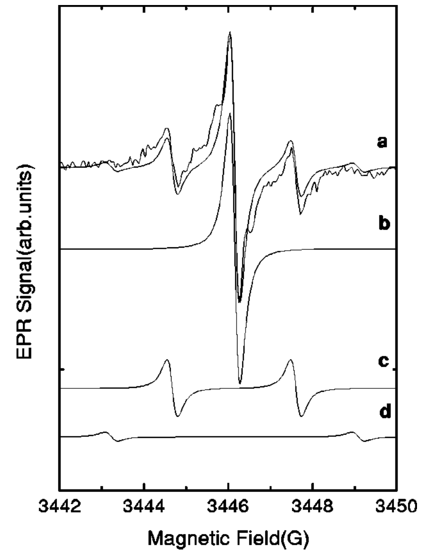

FIG. 2. Experimental spectrum (points) of the $V_{\mathrm{Si}}{}^{-}$ center in 6H-SiC and its decomposition in a central line (b) and a ^{29}Si doublet of 28% intensity ratio and 2.94 G splitting(c); the additional low intensity doublet (splitting 5.8 G) corresponding to the presence of two ^{29}Si atoms in the 2nd NN shell is equally given (d). The continuous line (a) shows the superposition of the three simulated spectra; $T=300\,\mathrm{K}$, $B\|c$.

tion is still missing. Most previous studies of ion-implantation-induced defects were performed by optical or electrical techniques, and the distinction between the defects generated in the trace and in the stopping range was not attempted. In principle the EPR technique is unable to distinguish between these regions either, since the entire volume of the sample is analyzed simultaneously. In order to overcome this difficulty we have chosen to apply high-energy proton implantation in this study, such that the incident protons will completely cross the sample and only trace defects will be generated.

EXPERIMENT

N-type nitrogen-doped $(2\times10^{17}\,\mathrm{cm}^{-3})$ (0001)-oriented 4H- and 6H-SiC substrate wafers ~300 μm thick were purchased from a commercial supplier (Cree Research, Durham, NC). The substrates were one side polished, 7° off-axis. The proton implantation was performed at the CERI irradiation facility (Center d'Etudes et de Recherches par Irradiation, CNRS, Orleans, France) under the following conditions: proton energy 12 MeV, current ~μA/cm^2, and substrate temperature $T<50\,°\mathrm{C}$, proton dose $(1,\ldots,8)\times10^{16}\,\mathrm{cm}^{-2}$. The projected range of 12-MeV protons in SiC is given by SRIM2000 as 666 μm, with a range straggle of 26 μm. The samples, of typical dimensions of $5\times5\,\mathrm{mm}^2$, were then analyzed by standard *X*-band EPR spectroscopy at 300 K and low temperature. The effective *g* factors were determined via measurements of the microwave frequency with a frequency meter and the magnetic field with a proton NMR probe. We estimate the precision to be ±0.0001. Absolute spin concentrations were obtained by comparison with an Al_2O_3:Cr standard sample purchased from the National Institute of Science and Technology (NIST). In order to enhance the precision with which defect numbers can be determined by the double integration of the EPR spectra, the total spectra were decomposed into their respective components by computer-assisted simulation, and the integration was performed on the component parts. The relative error is estimated to less than 5% with the exception of the $V_{\mathrm{Si}}{}^{0}$ $c1$ and $c2$ centers were due a strong overlap of other spectra an error of 20% is estimated.

RESULTS

6H-SiC samples

After the lowest dose of $1\times10^{16}\,\mathrm{cm}^{-2}$, the samples are electrically compensated at room temperature. The compensation can be deduced from the quality factor of the loaded cavity and is directly confirmed by the absence of a free-electron resonance signal at room temperature and the nitrogen donor spectrum at low temperature. It shows that for this proton dose deep acceptor defects have been predominantly generated such that $\mathrm{N}_{da}>\mathrm{N}_{d}+\mathrm{N}_{dd}-\mathrm{N}_{a}$, where N_{da}, are deep acceptors, N_{d} is the nitrogen doping, N_{a} is the residual acceptor (mainly B) concentration, and N_{dd} is the deep donor concentration. It corresponds to an effective carrier reduction rate of ~20 cm^{-1}.

Under thermal equilibrium conditions at 300 K, and for the lowest dose, the samples show three dominant EPR spectra. The first one (Fig. 2) is an isotropic spectrum with a *g* factor of 2.0032, a central line of peak to peak width of 0.25 G, and two sets of hyperfine lines: the first is a doublet of 2.94-G splitting, and an intensity ratio $I_{\mathrm{HF}}/I_{\mathrm{central}}=0.28$. At higher gain an additional doublet with a splitting of 5.8 G is observed. The second set of hyperfine lines is anisotropic and for a magnetic-field orientation $B\|[0001]$, is characterized (Fig. 3) by two doublets with splittings of 14.0 and 28.5 G; their intensity ratio relative to the central line is $I_{\mathrm{HP}}/I_{\mathrm{central}}=0.04$. This spectrum was already reported previously, and attributed to the negatively charged silicon vacancy V_{Si}^{-}.[19–21] The electron spin of this center, which could not directly be determined from the EPR spectrum was shown by electron nuclear double resonance measurements[20]

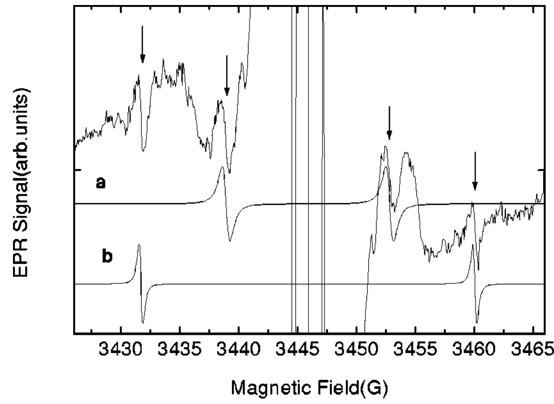

FIG. 3. EPR spectrum of the V_{Si}^- center taken at higher gain; in addition to the strong central part two hyperfine doublets with splittings of 28.5 G and 14.0 G are observed and simulated in (*a,b*); from their relative intensity they can be attributed to the interaction with 1 and 3 carbon nearest neighbor atoms respectively; $T = 300$ K, $B \| c$.

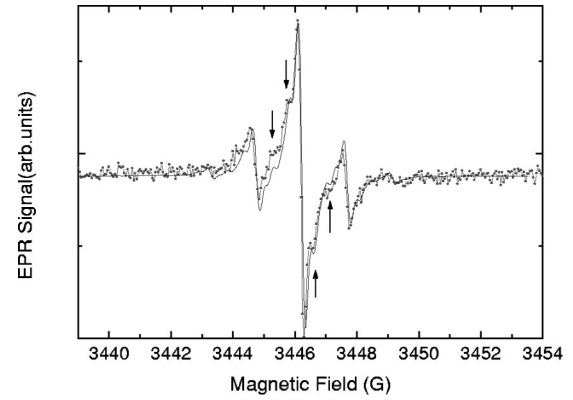

FIG. 4. Simulation(line) of the experimental spectrum (dots) of the negatively charged Si vacancy EPR spectrum in 6H-SiC assuming in addition to the 12 NNN Si hyperfine interaction an interaction with 12 C atoms of 1.72 G and 6 Si atoms of 0.65 G. The structures in the spectrum generated by the additional SHF interaction are indicated by arrows; $T = 300$ K, $B \| c$.

to be $S = \frac{3}{2}$, as expected for the $^4A_2$ ground state of the V_{Si}^- defect.[22] The two HF doublet systems correspond to the interaction with the four nearest-neighbor carbon atoms (^{13}C with $I = \frac{1}{2}$ isotopic abundance 1.1%) and the 12 next-nearest-neighbor NNN Si atoms (^{29}Si, $I = \frac{1}{2}$, abundance 4.7%). Contrary to the transition-metal-related and other intrinsic defects no site dependence of its EPR spectrum has been detected in any previous studies nor in this case.

The observation of an isotropic EPR spectrum for an $S = \frac{3}{2}$ center at a site of C_{3v} symmetry, and the absence of site sensitivity, is *a priori* surprising. In the related case of a negatively charged carbon vacancy in diamond, this situation has been analyzed, and the small effect of the crystal field on the zero-field splitting parameter D has been ascribed[23] to the large separation of the excited states with T_1 symmetry, which require strong electrical fields in order to render its effect observable in EPR. We have also recently observed[24] anisotropic V_{Si}^--related defects in 6H-SiC, they were formed after low-energy electron irradiation; we have attributed these centers to close V_{Si}^--Si_i Frenkel pairs. In the proton-implanted material studied here only the isolated silicon monovacancy V_{Si}^- is observed.

The high signal-to-noise ratio allows us to study in more detail the central part of the spectrum; if a low-magnetic-field modulation amplitude (<0.1 G) is employed, an additional weaker superhyperfine (SHF) structure is revealed. As shown in Fig. 4, the V_{Si}^- spectrum in the proton-implanted samples contains a structure between the central line and the 2.94-G doublet, which has not been reported in the previous studies, to our knowledge. This structure can be used to further refine the microscopic model of this defect: if the center is an isolated vacancy, the additional SHF structure can reasonably be expected to be due to the interaction with ^{29}Si and ^{13}C atoms in the third- and fourth-nearest-neighbor (NN) shell of the Si sites, which are composed of 12 C and six Si atoms respectively. We have thus performed a computer-assisted analysis of the shape of the central line. The simulation of the spectrum taking in consideration an additional interaction with 12 carbon third NN with a splitting of 1.72 G, and six silicon fourth NN's with a splitting of 0.65 G is shown in (Fig. 4). The fit is satisfying, and can be considered as an additional support for the isolated V_{Si} defect model.

From a double integration of the EPR spectrum and a comparison with the Cr^{2+} spectrum in the ruby standard sample, the absolute concentration of the V_{Si}^- defect in the $1 \times 10^{16}\,\mathrm{cm}^{-2}$ proton-irradiated sample is determined to $7 \times 10^{16}\,\mathrm{cm}^{-3}$. The negatively charged silicon monovacancy is thus one of the dominant trace defects after proton implantation with an introduction rate of 7 cm^{-1}.

If we extend the magnetic-field range at which the EPR spectra are studied, we observe (Fig. 5) two further spectra which for $B \| [0001]$ are each characterized by a doublet with splittings of 90.4 and 19.3 G, respectively. Their peak to peak linewidth of $\sim$3 G is much higher than the one of the V_{Si}^- center ($\Delta B_{pp} = 250$ mG) (see Table I). Both spectra are anisotropic, and show (Fig. 6) an angular variation characteristic for a spin $S = 1$ center with a purely axial field splitting. It is described by the expression

$$B = \frac{1}{g\mu_B}\left(h\nu \pm \frac{D}{2}[3(\cos\vartheta)^2 - 1]\right),$$

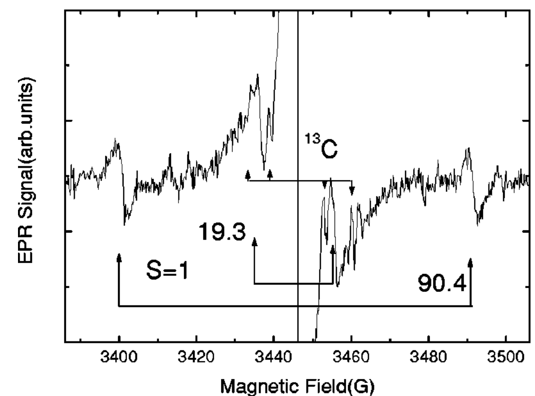

FIG. 5. EPR spectrum of 6H-SiC:N after a proton dose of $1 \times 10^{16}\,\mathrm{cm}^{-2}$; $T = 300$ K, $B \| c$. It shows two $S = 1$ doublet spectra with splittings of 90.4 G and 19.3 G and linewidths of 2.8 G as well as the sharp ^{13}C HF lines of the central V_{Si}^- line; $T = 300$ K, $B \| c$.

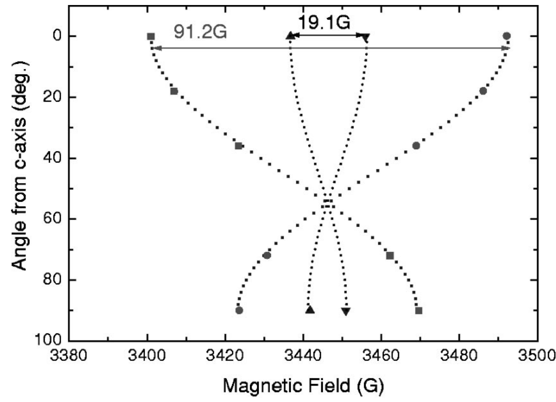

FIG. 6. Experimental (squares/triangles) and simulated (points) angular variation of the two $S=1$ centers in 6H-SiC; parameters $g_{iso}=2{,}0030$ and $D=42.8\times10^{-4}\ \mathrm{cm}^{-1}$ and $g_{iso}=2.0030$ and $D=9.1\times10^{-4}\ \mathrm{cm}^{-1}$; $T=300\ \mathrm{K}$, rotation plane (11–20).

with B the resonance field, g the Landé g factor, μ_B the Bohr magneton, $h\nu$ the microwave energy, D the zero-field splitting parameter, and ϑ the angle between the magnetic field B and the crystal c axis.

The complete angular variation of the outer doublet spectrum has been studied for a rotation of the magnetic field in the (11-20) (Fig. 6) and (0001) planes. The spin Hamiltonian parameters of this defect are spin $S=1$, $g_{iso}=2.0032\pm0.0004$, and $D=42.8\times10^{-4}\ \mathrm{cm}^{-1}$. The simulation of the angular variation with these parameters is superposed in Fig. 6. The second spin $S=1$ spectrum has only been analyzed for the orientations $B\|c$ and $B\perp c$, as the $V_{Si}{}^{-}$ spectrum strongly perturbs the analysis for intermediate orientations. It nevertheless allows one to estimate its parameters to $g_{\|c}=2.0032\pm0.0004$, $g_{\perp c}=2.0032\pm0.0004$, and $D=9\times10^{-4}\ \mathrm{cm}^{-1}$.

Two defects with very similar spin Hamiltonian parameters were reported previously in an EPR study of thermally quenched samples ($P3$,$P5$),[25] and more recently in an optically detected magnetic resonance (ODMR) study of electron irradiated n-type 6H-SiC[26] (see Table II). As the D parameters are identical within the experimental accuracy, we obviously observe the same defects as the previous authors. The slightly different g values observed by us and in Ref. 26 are probably due to the high linewidth of the spectra (>1 and 2.8 G respectively) which limit in our case the precision for the g-factor determination to $\Delta g=\pm0.0004$ as well as to the different measurement temperatures (2 K/300 K). The first authors[25] attributed the centers to vacancy pair defects, whereas Sörman *et al.*[26] attributed them to the neutral isolated silicon vacancy on the hexagonal and quasicubic lattice sites, respectively. The two quasicubic sites $c1$ and $c2$ cannot be distinguished for this defect. The authors at Ref. 25 were apparently misled in their defect model by an incorrect interpretation of the Si SHF interaction. It should be recalled that at that time the negatively charged silicon vacancy had not yet been identified. Sörman *et al.*[26] were able to analyze the Si SHF structure, the interpretation of which is main argument for the assignment of vacancy defects, quantitatively. For both $S=1$ centers it is characterized by an isotropic splitting of 2.9 G and an intensity ratio of the HF lines to the central line corresponding to that of a 12-Si-atom neighbor shell, i.e., the second-nearest-neighbor shell of a Si site. The assignment by Sörman *et al.* is also confirmed by the ^{13}C NN HF interaction, which was resolved in the first study.[25] The number of interacting first neighbors (1+3C atoms) and the principal values of the HF tensor of 26.6×10^{-4} and $13.6\times10^{-4}\ \mathrm{cm}^{-1}$, which are very close to those reported for the negatively charged Si vacancy, leave no doubt for the V_{Si} defect model. Due to the high linewidth of 2.8 G the ^{29}Si SHF structure is not resolved in our 300 K EPR spectrum, but leads only to a change in line shape. We consider the HF structure data as sufficiently strong evidence for the assignment of this spectrum to a Si monovacancy defect, and we will adapt this model in the following part of this paper.

The ground-state configuration of the neutral silicon vacancy in SiC has been the object of various calculations. In 6H-SiC the ground state of the undistorted neutral silicon vacancy $V_{Si}{}^{0}$ was predicted[22,27] to be a spin singlet ^{1}E state with an excited spin triplet $^{3}T_1$ state at 0.1, 0.2 eV; a diamagnetic ^{1}E state is of course not observable in an EPR experiment. The EPR study in this case would require a thermal or optically induced population of the first excited $^{3}T_1$ state. More recently, a paramagnetic spin $S=1$ ground state was also proposed for the $V_{Si}{}^{0}$ defect.[28,29] This raises the question of whether the spectrum observed by us and in Refs. 25 and 26 is a thermally populated excited state or the

TABLE I. Spin Hamiltonian parameters of the negatively charged silicon vacancy in 6H-SiC, Landé g-factor, ^{13}C hyperfine interaction tensor with the first nearest neighbors, ^{29}Si HF interaction constant with the 12 second nearest neighbors, ^{13}C hyperfine interaction tensor with the 12 third nearest neighbors, ^{29}Si HF interaction constant with the 6 fourth nearest neighbors, peak-to-peak linewidth of the EPR line.

g-factor	^{13}C HF(G) 4 1st nn	^{29}Si HF(G) 12 2nd nn	^{13}C HF(G) 12 3rd nn	^{29}Si HF(G) 6 4th nn	Width (G)	Ref.
2.0032	$A\|=28.8$ $A\perp=11.2$	2.94	1.75	0.72	0.25	This work
2.003	⋯	⋯	⋯			Schneider *et al.* (1993) Ref. 19
2.0015	$A\|=28.7$ $A\perp=11.5$	2.97				Wimbauer *et al.* (1997) Ref. 20
2.0030						Kawasuso *et al.* (1999) Ref. 21

TABLE II. 6H-SiC: Defect models, Landé g-factors, zero field splitting parameter D and observation temperature for the two spin $S=1$ defects observed here and the corresponding values for the $P3$,$P5$ defects observed by Vainer *et al.* and T_{V2a}, T_{V3a} centers reported by Sörman *et al.*, Ref. 26.

Defect model	g-factor	$D(10^{-4}\,\mathrm{cm}^{-1})$	T/K	Reference	comment
V_{Si}^0 Hexa.site	$g_{iso}=2.0032$	42.8	300,4	This work	EPR
V_{Si}^0 C1,c2 sites	$g_{iso}=2.0032$	9	300,4	This work	EPR
divacancy $V_{Si}-V_C$	$g\parallel=2.0026$ $g\perp=2.0031$	43	77	Vainer *et al.* (1981) 25	P3 EPR
divacancy $V_{Si}-V_C$	$g\parallel=2.0026$ $g\perp=2.0031$	9	77	Vainer *et al.* (1981) 25	P5 EPR
V_{Si}^0 Hexa.site	$g\parallel=2.0035$ $g\perp=2.0038$	42.8	2	Sörman *et al.* (2000) 26	T_{V2a} ODMR
V_{Si}^0 C1,c2 sites	$g\parallel=2.0037$ $g\perp=2.0026$	9.2	2	Sörman *et al.* (2000) 26	T_{V3a} ODMR

defect ground state. Sörman *et al.*[26] and Wagner *et al.*[30] attributed the spectrum to an excited state of ${V_{Si}}^0$; however, as in an ODMR experiment the measurement are not done under thermal equilibrium conditions the distinction between ground and excited states is more difficult than in an EPR experiment where the measurements can be done under thermal equilibrium conditions. To further investigate this issue, we have measured the EPR spectrum of ${V_{Si}}^0$ over the whole 300–4 K temperature range. We find, in particular, that the spectrum is still observable with unchanged parameters at 4 K, which excludes its attribution to an excited state at 0.1 eV or higher energy. We thus deduce from the low-temperature measurements that the ${V_{Si}}^0$ center has a paramagnetic spin-1 ground state. More details of this spectrum will be published elsewhere.

The concentrations of the neutral ${V_{Si}}^0$ centers (h, $c1$, and $c2$) after a $1\times10^{16}\,\mathrm{cm}^{-2}$ proton dose have been determined to ${V_{Si}}^0(h)=6\times10^{16}\,\mathrm{cm}^{-3}$ and ${V_{Si}}^0(c1,c2)=6\times10^{16}\,\mathrm{cm}^{-3}$, which are of comparable magnitude to that of the ${V_{Si}}^-$ center. For higher proton doses the four silicon-vacancy-related defects ${V_{Si}}^-$, ${V_{Sih}}^0$, ${V_{Sic1}}^0$, and ${V_{Sic2}}^0$ increase in intensity without any change in the spin Hamiltonian parameters. The variation of the ${V_{Si}}^-$, ${V_{Sih}}^0$, and ${V_{Sic1,c2}}^0$ concentrations as a function of proton dose is given in Fig. 7. The precision with which the concentration of ${V_{Sic1,c2}}^0$ can be determined is lower due to the overlap with the strong ${V_{Si}}^-$ spectrum; the possible relative error is estimated to 20%. Their concentration is close to that of the hexagonal site center. Thus for a proton dose of $1\times10^{16}\,\mathrm{cm}^{-2}$ we observe a total concentration of $1.9\times10^{17}\,\mathrm{cm}^{-3}$ silicon vacancies.

The silicon vacancy concentration predicted from the SRIM simulations for this proton dose is $3.7\times10^{18}\,\mathrm{cm}^{-3}$, which is 20 times higher than the one observed. This discrepancy can not be attributed to a ''hidden'' diamagnetic fraction of V_{Si}; as both the 0 and 1 charge states are simultaneously observed. We conclude thus that only a small fraction of the primary silicon vacancies persists at 300 K. The most probable process for the vacancy reduction is interstitial/vacancy interactions, which are not taken into account in the SRIM simulations. This recombination is known to be efficient at room temperature in n-type Si.[31] In electron irradiated n-type 6H-SiC a room-temperature annealing stage has also been observed and attributed to a partial recombination of interstitial/vacancy pairs.[32]

If the electrical compensation of the proton-implanted samples is dominated by the silicon monovacancy defects, which is the case according to our results, the simultaneous observation by EPR of the negatively charged silicon vacancy and the neutral silicon vacancy is not unexpected (see Table III). The V_{Si} defect, which introduces different levels in the forbidden gap for both negatively and positively charge states, can compensate both donor and acceptor

TABLE III. 4H-SiC: defect models, Landé g-factors, zero field splitting parameter D and observation temperature for the two spin $S=1$ defects observed in this work and the corresponding values for the T_{V2a},T_{V2b} centers reported by Sörman *et al.*, Ref. 26.

Defect model	g-factor	$D(10^{-4}\,\mathrm{cm}^{-1})$	T/K	Reference	comment
V_{Si}^0 Hexa.site	$g\parallel=2.004$ $g\perp=2.004$	23.2	2	Sörman *et al.* (2000) 26	T_{V2a} ODMR
V_{Si}^0 Cubic site	$g\parallel=2.004$ $g\perp=2.004$	12.1	2	Sörman *et al.* (2000) 26	T_{V2b} ODMR
V_{Si}^0 Hexa.site	$g_{iso}=2.0032$	22	300	This work	EPR
V_{Si}^0 Cubic site	$g\parallel c=2.0032$	13	300	This work	EPR

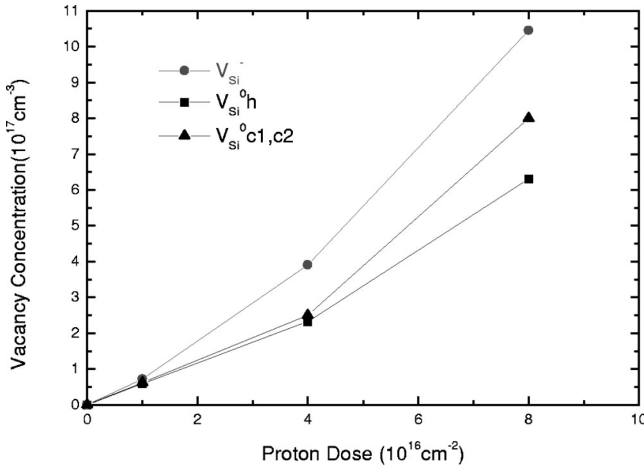

FIG. 7. Volume concentration of the negatively charged silicon vacancy (dots) and the neutral silicon vacancy on the hexagonal (squares) and quasicubic (triangles) sites in n-type 6H-SiC as a function of proton dose; $T=300$ K, proton energy 12 MeV; the lines are a guide for the eye.

dopants. In n-type doped material, it will pin the Fermi level on the $-/0$ level if its concentration $[V_{Si}]>[N]$; in our samples we observe after the lowest $1\times10^{16}\,\mathrm{cm}^{-2}$ proton dose a total V_{Si} concentration of $1.9\times10^{17}\,\mathrm{cm}^{-3}$, whereas the nominal nitrogen concentration has been given to $[N]=2\times10^{17}\,\mathrm{cm}^{-3}$. This can be considered a good agreement. Nevertheless, the actual situation can be expected to be more complicated: the concentration of negatively charged $[V_{Si}^-]=0.7\times10^{17}\,\mathrm{cm}^{-3}$ should in this simplest case-exclusive compensation by V_{Si}^- be equal to the donor concentration, which is not the case. Clearly, additional electron traps are present in the samples.

n-type 4H-SiC

Previous EPR studies on intrinsic and impurity-related defects have shown that the defect parameters in the 4H polytype are very close to those in the 6H-SiC. The principal difference is the smaller number of nonequivalent lattice sites: in 4H we have only one quasicubic site and one hexagonal site. In Fig. 8 we show the EPR spectrum observed in

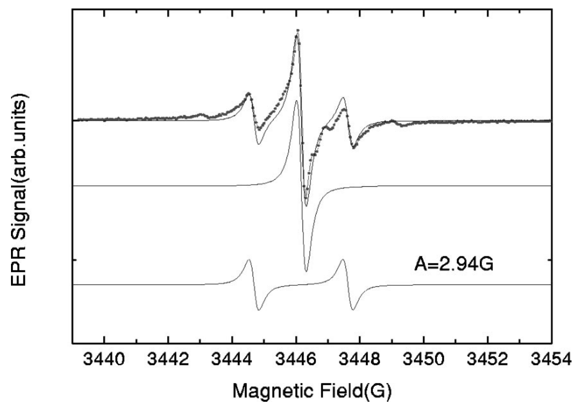

FIG. 8. Experimental EPR spectrum (points) of the V_{Si}^- center in n-type 4H-SiC and its decomposition in a central line and a ^{29}Si doublet of 28% intensity ratio and 2.94 G splitting. The continuous line shows the superposition of the two simulated spectra; $B\|c$, $T=300$ K; proton dose $4\times10^{16}\,\mathrm{cm}^{-2}$.

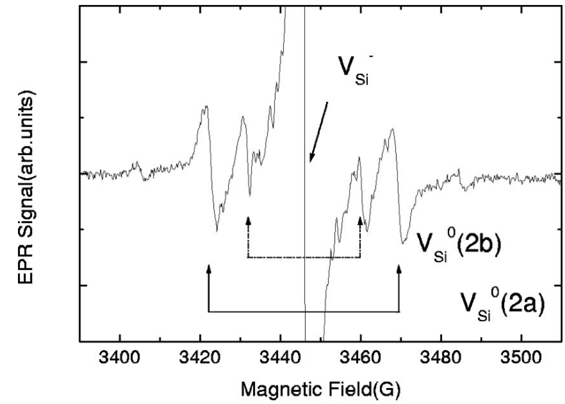

FIG. 9. EPR spectrum of 4H-SiC:N after a proton dose of $1\times10^{16}\,\mathrm{cm}^{-2}$; $T=300$ K, $B\|c$. It shows two $S=1$ doublet spectra with splittings of 46.7G(2a) and 28.5G(2b) as well as ^{13}CHF lines from the central V_{Si}^- line.

the 4H sample after a proton dose of $4\times10^{16}\,\mathrm{cm}^{-2}$. As expected, we observe an isotropic spectrum of the negatively charged silicon monovacancy characterized by a g factor of 2.0030 and a ^{29}Si second NN-HF splitting of 2.94 G. However, as in the case of 6H-SiC, an additional substructure with a smaller splitting is visible. The concentration of the V_{Si} defect is determined to $4\times10^{17}\,\mathrm{cm}^{-3}$.

At higher gain two additional spin $S=1$ centers (Fig. 9) are observed. They are characterized by isotropic g factors of $g=2.0030$ and zero-field splitting parameters $D=22\times10^{-4}$ and $13\times10^{-4}\,\mathrm{cm}^{-1}$, respectively. These centers were also reported previously,[26] and have been attributed to the neutral silicon monovacancy centers on the hexagonal and quasicubic sites. The apparent linewidth of the two $S=1$ spectra are different (2.9 G/1.5 G), and, given the small difference between the positions of the T_{V2a} and T_{V1b} spectra, the spectrum attributed to T_{V1a} could in fact be a superposition of the T_{V2a} and T_{V2b} spectra, which in this case must be of equal intensity. The T_{V1a} spectrum corresponding to the cubic site, which is characterized[26] by a very small zero-field splitting of $6.6\times10^{-4}\,\mathrm{cm}^{-1}$, cannot be detected due to the strong overlap of the central V_{Si}^- spectrum. The respective concentrations of the centers are 15×10^{17} and $5\times10^{17}\,\mathrm{cm}^{-3}$. We thus observe a very similar situation in n-type 4H and 6H-SiC, in which both the silicon vacancy in the neutral and negative charge states are observed as the dominant intrinsic trace defects generated by proton irradiation with the same introduction rates. We have further investigated the thermal stability of the V_{Si} defects in the 4H polytype (Fig. 10). Samples have been annealed at 900 °C and at 1100 °C. After the 900 °C anneal both the neutral and negatively charged V_{Si} are no longer observed. An anisotropic EPR spectrum [Fig. 10(b)] of low intensity is still present; it has not yet been identified. The spin density has, however, been strongly reduced. After an 1100 °C anneal this spectrum is also annealed out [Fig. 10(c)], and the samples recover an n-type conductivity.

DISCUSSION

In this EPR study we have identified the microscopic structure of the paramagnetic defects induced by proton im-

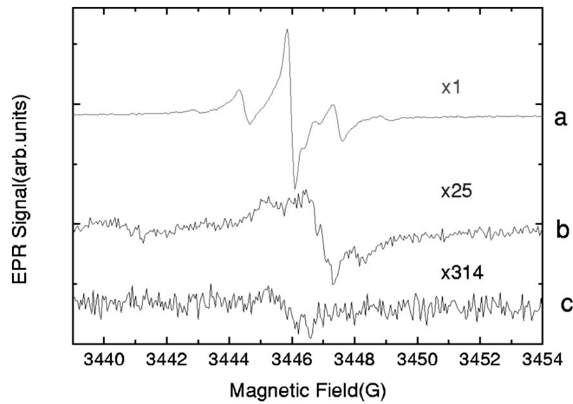

FIG. 10. EPR spectra of 4H-SiC:N after a proton dose of $1\times10^{16}\,\mathrm{cm}^{-2}$; $T=300\,\mathrm{K}$, $B\|c$. (a) as implanted, (b) after a 900 °C anneal, (c) after a 1100 °C anneal; the gain has been multiplied in (b) and (c) by 25 and 314 respectively.

plantation in the trace region: the three main paramagnetic defects observed in 6H and 4H polytypes are all attributed to the Si monovacancy defect on quasicubic and hexagonal lattice sites; in the whole proton dose range studied the Si vacancy is simultaneously observed in the two charge states $-/0$. The defect models had be established from the quantitative analysis of the HF and SHF structures.

The negatively charged $V_{\mathrm{Si}}{}^{-}$ has been identified from its known spin Hamiltonian parameter of $S=\frac{3}{2}$, its isotropic g value of $g=2.0032$, and the resolved hyperfine structure with four carbon nearest neighbors, and 12 equivalent silicon next-nearest neighbors. The isotropic character of the SHF interaction and g tensors are in agreement with the model of an isolated monovacancy defect. In fact, the only known silicon vacancy complex $V_{\mathrm{Si}}{}^{-}-X$, attributed to a close Si Frenkel pair, is characterized by modified spin Hamiltonian parameters with an anisotropic g tensor and a resolved zero-field splitting. The spatial separation of the primary vacancy/interstitial pair is expected under our irradiation conditions as energies largely above the displacement threshold energy of $\sim$24 eV are transmitted in 82% of the elastic collisions.

The spin-1 centers observed in our study can also clearly be attributed to the isolated silicon monovacancy in the neutral charge state. The defect model was previously established by Sörman *et al.*[26] in electron-irradiated SiC and based on the characteristic SHF interaction with the 12 next-nearest-neighbor Si atoms; with a value (2.6 G) close to the one of the negatively charged silicon vacancy (2.94 G), and is in agreement with the nearest-neighbor carbon HF interaction tensor reported in Ref. 25. Our simultaneous observation of the $V_{\mathrm{Si}}{}^{-}$ and $V_{\mathrm{Si}}{}^{0}$ centers under thermal equilibrium conditions and their similar concentration variation with proton dose fully confirm the defect model.

The silicon vacancy concentrations observed are however surprising. From the SRIM calculations shown above in Fig. 1, we deduce that each proton generates on average 12 displacement collisions with 1 replacement in the 300-μm-thick sample, leaving 11 primary vacancies, distributed between Si and C sites in the ratio 1.2:1. However, the observed introduction rate of the V_{Si} monovacancy defect is only 5% of this value. Analysis of the collision cascades obtained by the SRIM calculation shows that in the 300-μm-thick irradiated target 18% of the vacancies result from collisions in which the incident proton displaces only one atom—i.e., there is no cascade and in 82% more than one atom is displaced in the collision. Assuming even the extreme hypothesis that all vacancies produced in cascades of two or more atoms end up in configurations other than the isolated V_{Si}, we still observe only 29% of the vacancy concentration expected from SRIM. These results indicate that monovacancy annihilation processes operating at room temperature have to be considered. Possible processes are vacancy association (multivacancies, V_{Si}-dopant complex formation) or V_{Si} annihilation by recombination with Si or C interstitials. However, the lowest reported vacancy annealing stages, which were measured in electron-irradiated 6H-SiC, lie well above room temperature with $\sim$300 °C for the V_{C} vacancy and 750 °C for the V_{Si} vacancy. From these results we expect the vacancies not to be sufficiently mobile at room temperature to form multivacancies or V_{Si}-dopant complexes. This leaves as the most probable model vacancy interactions with mobile interstitials,[32] which can lead either to complete annihilation ($V_{\mathrm{Si}}+I_{\mathrm{Si}}\rightarrow \mathrm{Si}_{\mathrm{Si}}$) and/or antisite formation ($V_{\mathrm{Si}}+I_{\mathrm{C}}\rightarrow C_{\mathrm{Si}}$). An indication for the formation of antisite defects in 6H-SiC has been obtained from positron annihilation measurements in 2-MeV electron irradiated n-type material; the high concentrations of shallow positron traps, which were detected in addition to vacancy defects, have been tentatively attributed to antisite defects.[33]

The nonobservation of any carbon vacancy (V_{C})-related defect is unexpected. According to the SRIM calculations comparable V_{C} and V_{Si} defect concentrations have been formed in the collision processes. Up to now only one V_{C}-related paramagnetic defect, attributed to the positively charged monovacancy, has been reported. This defect has been studied in electron-irradiated p-type material,[34,35] and can be observed up to room temperature.[24] The spectrum is definitely not observed in our n-type samples after proton implantation. It should be recalled that in the case of 3C-SiC, which has been previously studied in more detail,[11] the V_{C}^{+} center (named T5) has also only been observed in p-type material. *A priori*, different reasons could be evoked for its nonobservation in n-type doped material such as a configurational instability or more simply a diamagnetic (0, 2+) charge state. The particular charge state of the V_{C} defect under thermal equilibrium conditions will of course depend on the Fermi-level position, which is in general modified during the irradiation. As we observe for all proton doses between 1 and $8\times10^{16}\,\mathrm{cm}^{-2}$, the neutral and negatively charged silicon vacancy simultaneously in thermal equilibrium the Fermi level does not move within this dose range, and is pinned by the $-/0$ level of V_{Si}. Considering the Fermi-level/charge-state correlation, two situations could give rise to a diamagnetic V_{C} ground state corresponding to the 0 and 2+ charge states: (i) the 0/+ level of V_{C} is situated below the $-/0$ level of V_{Si}, or if its $+/2+$ level lies above the $V_{\mathrm{Si}}-/0$ level.

A further insight in the vacancy level positions can be obtained from recent deep-level transient spectroscopy results[12,36] in n-type 6H-SiC; in the first study[12] the electron traps introduced by 2-MeV electron and 300-keV deuterium and hydrogen irradiations have been assessed. Three groups of levels have been detected at $E_C-0.62/0.64\,\mathrm{eV}$, E_C

-0.51 eV, and $E_C-0.34/0.41$ eV. Based on their annealing stages at 300 and 700 °C, they were attributed to carbon- and silicon-vacancy-related defects: two levels at $E_C-0.62/0.64$ eV was tentatively associated with the silicon vacancy and a level at $E_C-0.51$ eV with the carbon vacancy. Two additional levels at $E_C-0.34/0.41$ eV have been assigned to a different charge state of the carbon vacancy. Hugonnard-Bruyère *et al.*[36] equally studied the defects introduced by 50- and 120-keV proton implantation. In this study substrates with similar doping concentrations $[(1-2)\times 10^{17}\,\mathrm{cm}^{-3}]$ submitted to similar proton doses ($3\times 10^{15}\ldots 7\times 10^{16}\,\mathrm{cm}^{-2}$), as used here, have been studied. In the as implanted state—corresponding to our experimental situation—two electron traps with activation energies of $E_C-0.65$ and $E_C-0.35$ eV have been detected. The first corresponds to the $Z1/Z2$ center, whereas the second is the so-called P center. A coherent picture with our EPR results is obtained if the $E_C-0.62/0.64$-eV levels, and thus the $Z1/Z2$ center, are attributed to the $-/0$ states of the silicon monovacancy at the quasicubic and hexagonal lattice sites, respectively. At a first look this assignment might seem contradictory to the reported temperature dependence of the $Z1/Z2$ center, which is known to have a thermal stability up to 2000 °C,[37] whereas the silicon vacancy is known to anneal in the 750 °C range. However, whereas the irradiation-induced V_{Si} effectively anneals at 750 °C, it has been shown that the same center ($P2,P5_-$) is also generated by high-temperature annealing,[25] which represents a different physical situation. The high resistivity at room temperature of our samples after proton irradiation is in agreement with the assignment of the $E_C-0.62/0.64$-eV levels to the $-/0$ level of V_{Si}. The nonobservation of the carbon vacancy would imply that the $E_C-0.51$-eV carbon vacancy level should be assigned to the double donor state $+/2+$ of this center, and the two higher states to the $0/+$ charge states of V_C. As the concentration of the negatively charged V_{Si} after the highest proton dose is higher than the initial n-type doping, it follows that the proton implantation must also have created additional donor defects, which were not observed in EPR. The positively charged V_C center is a natural candidate for the donor defect.

CONCLUSION

The dominant intrinsic point defects in the trace region of proton implanted n-type 4H- and 6H-SiC have been identified as silicon monovacancies on hexagonal and cubic sites. The silicon monovacancy defect, which is introduced with an introduction rate of 19 cm^{-1}, pins the Fermi level in the as-implanted state. Comparison with previously published electrical measurements seems to indicate that the $Z1/Z2$ center corresponds to the V_{Si} center in the $-/0$ charge states. The lower silicon vacancy concentration, as compared to that expected from SRIM simulations, indicates a vacancy annihilation process—probably by due to interstitial recombination—already operating at 300 K. Thus the final vacancy concentration is expected to depend strongly on the implantation conditions. The neutral silicon vacancy on both the hexagonal and quasicubic sites has a paramagnetic groundstate in 4H- and 6H-SiC. The strong electrical compensation, which is observed after proton implantation with a dose of some $10^{16}\,\mathrm{cm}^{-2}$, can be eliminated by a 1100 °C anneal.

ACKNOWLEDGMENT

We thank M. F. Barthe and L. Henry from the CERI (CNRS/Orleans, France) for the proton implantation, and L. DiCioccio and E. Hugonnard-Bruyère from LETI (Grenoble) for support of this work. G. B. acknowledges support by the Hungarian OTKA Grant No. T032029.

[1] W. Skorupa, V. Heera, Y. Pacaud, and H. Weishart, Nucl. Instrum. Methods Phys. Res. B **120**, 114 (1996).

[2] V. Heera and W. Skorupa, in *Materials Modification and Synthesis by Ion Beam Processing*, edited by O. E. Alexander, N. W. Cheong, B. Park, and W. Skorupo, MRS Symposia Proceedings No. 438 (Materials Research Society, Pittsburgh, 1997), p. 241.

[3] L. DiCioccio, Y. Le Tiec, F. Letertre, C. Jaussaud, and M. Bruel, Electron. Lett. **32**, 1144 (1996).

[4] S. Greulich-Weber, Phys. Status Solidi A **162**, 95 (1997).

[5] J. Baur, M. Kunzer, and J. Schneider, Phys. Status Solidi A **162**, 153 (1997).

[6] K. F. Dombrowski, M. Kunzer, U. Kaufmann, J. Schneider, P. G. Baranov, and E. N. Mokhov, Phys. Rev. B **54**, 7323 (1996).

[7] A. L. Barry, B. Lehmann, D. Fritsch, and D. Bräunig, IEEE Trans. Nucl. Sci. **38**, 1111 (1991).

[8] J. F. Ziegler, J. P. Biersack, and U. Littmamark, *The Stopping and Range of Ions in Solids* (Pergamon, Oxford, 1985); J. F. Ziegler (unpublished).

[9] W. J. Choyke and L. Patrick, Phys. Rev. B **4**, 1843 (1971).

[10] W. J. Choyke, Inst. Phys. Conf. Ser. **31**, 58 (1977).

[11] H. Itoh, M. Yoshikawa, I. Nashiyama, H. Okumura, S. Misawa, and S. Yoshida, J. Appl. Phys. **77**, 837 (1995).

[12] M. O. Aboelfotoh and J. P. Doyle, Phys. Rev. B **59**, 10 823 (1999).

[13] D. Aberg, A. Hallen, and B. G. Svenson, Physica B **273–274**, 672 (1999).

[14] G. Brauer, W. Anwand, P. G. Coleman, A. P. Knights, F. Plazola, Y. Pacaud, W. Skorupa, J. Störmer, and P. Willutski, Phys. Rev. B **54**, 3084 (1996).

[15] G. Brauer, W. Anwand, P. G. Coleman, J. Störmer, F. Plazola, J. M. Campillo, Y. Pacaud, and W. Skorupa, J. Phys.: Condens. Matter **10**, 1147 (1998).

[16] R. C. Barklie, M. Collins, B. Holm, Y. Pacaud, and W. Skorupa, J. Electron. Mater. **26**, 137 (1997).

[17] E. A. Chowdhury, T. Seki, T. Izumi, H. Tanaka, and T. Hara (unpublished).

[18] E. Hugonnard, F. Letertre, L. DiCioccio, H. J. von Bardeleben, J. L. Cantin, T. Ouisse, T. Billon, and G. Guillot (unpublished).

[19] J. Schneider and K. Maier, Physica B **185**, 199 (1993).

[20] T. Wimbauer, B. K. Meyer, A. Hofstâtter, A. Scharmann, and H. Overhof, Phys. Rev. B **56**, 7384 (1997).

[21] A. Kawasuso, H. Itoh, D. Cha, and S. Okada (unpublished).

[22] F. P. Larkins and A. M. Stoneham J. Phys. C **3**, L112 (1970).
[23] J. E. Lowther and A. van Wyk, Phys. Rev. B **49**, 11 010 (1994).
[24] H. J. von Bardeleben, J. L. Cantin, L. Henry, and M. F. Barthe, Phys. Rev. B (to be published).
[25] V. S. Vainer and V. A. Il'in, Fiz. Tverd. Tela (Leningrad) **23**, 3659 (1981) [Sov. Phys. Solid State **23**, 2126 (1981)].
[26] E. Sörmann, N. T. Son, W. M. Chen, O. Kordina, C. Hallin, and E. Janzen, Phys. Rev. B **61**, 2613 (2000).
[27] P. Deak, J. Miro, A. Gali, L. Udvardi, and H. Overhof, Appl. Phys. Lett. **75**, 2103 (1999).
[28] J. Furthmuller, A. Zywietz, and F. Bechstedt, Mater. Sci. Eng., B **61–62**, 244 (1999).
[29] L. Torpo, R. M. Nieminen, K. E. Laasonen, and S. Pöykkö, Appl. Phys. Lett. **74**, 221 (1999).
[30] Mt. Wagner, E. Sörman, C. Hallin, J. L. Lindström, W. M. Chen and E. Janzen, in *Proceedings of the 20th International Conference on Defects in Semiconductors*, edited by C. van de Walle and W. Walukiewicz, North Holland, Elsevier (1999), page 102.
[31] B. G. Svenson, C. Jagadish, A. Hallen, and J. Lalita, Nucl. Instrum. Methods Phys. Res. B **106**, 183 (1995).
[32] A. Kawasuso, H. Itoh, T. Ohshima, K. Abe, and S. Okada, J. Appl. Phys. **82**, 3232 (1997).
[33] A. Polity, S. Huth, and M. Lausmann, Phys. Rev. B **59**, 10 603 (1999).
[34] N. T. Son, W. M. Chen, J. L. Lindström, B. Monemar, and E. Janzen, Mater. Sci. Forum **264–268**, 599 (1998).
[35] D. Cha, H. Itoh, N. Morishita, A. Kawasuso, T. Oshima, Y. Watanbe, J. Ko, K. Lee, and I. Nashiyama, Mater. Sci. Forum **264–268**, 615 (1998).
[36] E. Hugonnard-Bruyère, V. Lauer, G. Guillot, and C. Jaussaud, Mater. Sci. Eng., B **61–62**, 382 (1999).
[37] T. Dalibor, C. Peppermüller, G. Pensl, S. Sridhara, R. P. Devaty, W. J. Choyke, A. Itoh, T. Kimoto, and H. Matsunami, Inst. Phys. Conf. Ser. **142**, 517 (1996).